Observed Evolution of Tropical Deep Convective Events and Their Environment

STEVEN C. SHERWOOD AND RALPH WAHRLICH

School of Earth Sciences, Victoria University of Wellington, Wellington, New Zealand

(Manuscript received 18 February 1998, in final form 28 August 1998)

ABSTRACT

Using a compositing technique, the temporal progression of tropical convective systems and the mean atmospheric state in their vicinity is constructed from a time series of geostationary satellite and operational rawinsonde data. The technique establishes the stage in the life cycle of convection prevailing at a given place and time, by a simple objective method using time series of satellite brightness temperature (T_b) histograms collected from a region surrounding the site. Soundings are classified according to their placement in the convective life cycle, and composites formed that represent the areal-mean state of the convecting atmosphere at each stage, for several scales of horizontal averaging.

The temporal structure found here for the mesoscale-mean atmosphere closely resembles existing observations of the horizontal structure of a tropical squall line, albeit with certain reductions in amplitude and stabilization rate. This supports the generality of previous findings that the physical mechanisms documented for squall line systems are characteristic of other forms of tropical convection, and quantifies their imprint on thermodynamic mean fields at large spatial scales. The results show an instability decay time during convection of about 3 h at the 120-km horizontal scale. This time grows with scale, as does the duration of the mature stage of convection, which is of similar magnitude. The results also show a column-integrated loss of water vapor and moist static energy following convection. These results may be of use in model validation and theoretical treatments of convective interaction with dynamics.

1. Introduction

Convective phenomena dominate the description of tropical weather and climate. An oft discussed convective entity is the so-called mesoscale convective system (MCS), which appears as a connected blob of convective activity or cloud cover in satellite imagery but is seen to contain a wealth of internal structure when observed by radar or in situ. An MCS initiates, grows to sizes of order 10^4–10^6 km^2, and then decays, with a lifetime on the order of one day. This paper describes the evolution of convective activity and its mean-field environment on the length scale typical of an MCS by means of a compositing technique, offering a different perspective from previous studies. While many such studies have focused on spatial structure, we focus instead on the temporal behavior of the spatially averaged state (which we sometimes call the ''environment,'' though this term is normally attached to the preconvective or surrounding air masses only). The results should be directly applicable to the theory and modeling of scale interaction and climate.

Tropical weather phenomena occupy a spectrum of length and time scales—ranging from convective drafts to the overturning Hadley and Walker circulations—in which the MCS assumes an intermediate position. The various scales interact, which has led to the concept of convective ''organization.'' The MCS itself, in which multiple convective cells tend to be arranged along the edge of a mesoscale disturbance, is only one form of organization. Other examples include synoptic-scale easterly waves, which have been found to modulate convective activity and rainfall (Reed and Recker 1971; Houze and Betts 1981), superclustering of systems (Lau et al. 1989), and, on longer temporal and spatial scales, the tropical intraseasonal oscillation (Madden and Julian 1972). Understanding of these is still developing. Chen et al. (1996) give a recent account of convective behavior over the tropical western Pacific as observed during the Tropical Ocean Global Atmosphere (TOGA) Coupled Ocean–Atmosphere Response Experiment (COARE), including further discussion of convective organization.

The source of such forms of organization must lie in the interaction between convection and environmental state variables, so a key to understanding them is to learn how convective effects below a given length scale respond to the environmental variables averaged over that scale. If this is understood quantitatively on the smallest scale accessible to a numerical circulation mod-

Corresponding author address: Dr. Steven Sherwood, NASA/Goddard Space Flight Center, Mail Code 916, Greenbelt, MD 20771.
E-mail: sherwood@zephy.gsfc.nasa.gov

el, then that model may in principle be used to simulate behavior (and feedbacks) at larger scales. Unfortunately, no widely accepted theory exists for explaining convective behavior on the necessary scales, which in present-day, global models are of the same order as the size of a typical MCS.

A wealth of data exists on the structure of tropical systems, obtained mainly from field programs over the past three decades. Squall lines have been the most studied. These have a recurring structure that includes a narrow convective line, usually propagating into the environment, and a broad wake. Composite sounding analyses of these components show clear differences between them (Betts et al. 1976; Fitzgarrald and Garstang 1981; Barnes and Sieckman 1984), at least in the boundary layer. Convection assumes many other, less organized forms, which have also been documented and show many similarities to the squall line systems. These and other findings prior to COARE are summarized by Houze (1989).

Unfortunately, it is not clear how to put these composite profiles to use in our efforts to understand large-scale behavior. There is little doubt that convective systems have an impact at large scales that extends far beyond the convective part of the system in both space and time (Jabouille et al. 1996). The main problem is that few, if any, models can simulate the features and/or physics of an MCS and large-scale behavior at the same time. Another problem is that the features of the most studied systems may not be fully representative of all important convection. Some composite analyses of the thermodynamic states of convecting atmospheres have been performed without limiting attention to organized systems or to the boundary layer, but most of these only characterize ''clear'' and ''cloudy'' conditions, with no information on spatial or temporal structure (e.g., Mapes and Houze 1992; Fu et al. 1994). Temporal information is important, because our understanding of the interactions must be process oriented and have a correct causal basis; information distinguishing causes from their effects may most easily be obtained observationally through high temporal resolution.

One study that does examine a time series involving many convective events is the Global Atmosphere Research Program (GARP) Atlantic Tropical Experiment (GATE) array study of Frank (1978). He found a composite structure resembling that of the easterly wave but noted that the convective events were initiated by mesoscale disturbances. Though he formed separate sounding composites for squall and nonsquall systems, no significant differences appeared except in wind shear. The number of systems available during the experiment was sufficient only to provide somewhat rough, but informative, composites. A number of time series and compositing studies of surface and/or boundary layer variables have also been performed using various types of gound-based instrumentation (Gaynor and Mandics 1978; Young et al. 1995).

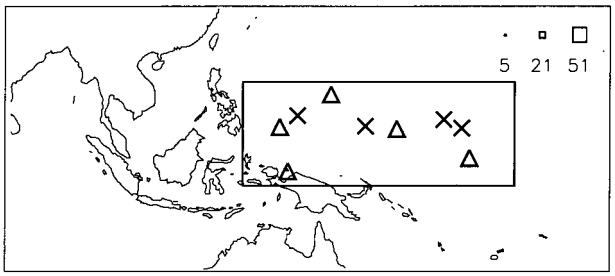

FIG. 1. The area observed for this study is the rectangular region bounded by 127°E, 178°W, 16°N, and 4°S. The crosses and triangles show the locations of rawinsonde stations, with crosses indicating reef/small island stations [see section 4b(4)]. The squares at the upper right show three box sizes used in section 4c with *L*, the side length in GMS pixels, indicated underneath each one.

The present study attempts to improve the situation by forming estimates of the mean conditions over a region of specified size, in convective atmospheres hour by hour as the convection develops. Various scales are observed, but no attempt is made to distinguish between different locations within the systems, between forms of convective organization, or between behavior during different seasons, all subjects that are better served by previous efforts. It turns out that the characteristics of an air mass still change rapidly as it begins to convect, even when averaged over areas of over 10^5 km^2 (though not as rapidly as what one observes immediately behind a narrow squall line). This and other composite results are presented in section 4. First, by carefully tracking a number of systems, it is shown in section 3 that that the principles used in the compositing method are valid. The issue of how convective behavior responds to prevailing large-scale conditions will be examined more carefully in a forthcoming paper.

2. Data

Measurements of the thermodynamic state of the atmosphere are obtained from operational radiosonde data retrieved from the National Center for Atmospheric Research Data Support System. Infrared imagery from the Japanese Geostationary Meteorological Satellite (GMS), archived at Victoria University of Wellington, Wellington, New Zealand, is used to locate convective activity. The area examined in this study (shown in Fig. 1) lies over the western Pacific ''warm pool,'' where convection occurs in abundance. The study covers 18 months from January 1995 to June 1996.

The study region encloses nine regularly operating upper-air stations (Koror, Biak, Yap, Guam, Truk, Ponape, Kwajalein, Majuro, and Tarawa), which launch sondes twice per day (soundings at Biak and Tarawa are often missing). The soundings in this study were interpolated to a regular 20-hPa grid and subjected to quality control procedures described in Sherwood (1996) to remove serious errors due to problems such as sensor icing and imperfect data transmission. Unfortunately, a va-

riety of errors remain in the soundings (Elliot and Gaffen 1991; Zipser and Johnson 1998). The present work is resistant to random sounding errors and station-dependent biases, but not to biases that may result from the effects of clouds and precipitation on the sensors. We have no way of correcting for any such effects and must hope that they are small.

The objectives of this study require close temporal matching of sounding and satellite observations. The study region is in full view of the *GMS-5* satellite, whose IR1 channel radiances are used to indicate convective activity. Over the region used for this study, a pixel footprint ranges from about 5 to 6.5 km. The temporal resolution is 1 h, with scan times at approximately 30 min past the hour. Four additional scans are available per day but were used only in section 3. Note that the scans begin at the north, reaching the equatorial region approximately 10 min after the nominal scan time; similarly, the radiosonde requires about an hour to reach the tropopause, and after 10 min has reached approximately the 800–700-hPa level. The scan and launch times shall be regarded as comparable observation times of the respective observing platforms. Though soundings are not always launched at their nominal launch time, it is hoped that most are launched quite close to this time.

The GMS IR1 radiances are expressed as effective radiating temperatures, or brightness temperatures T_b. Interpretation of these will be discussed in the next section, after a brief overview of previous observations of tropical convective systems.

3. A satellite view of the life of a tropical MCS

a. Review

Mesoscale convective systems generally consist of a group of deep cumulonimbus cells, connected by extensive stratiform cloud decks in the middle to upper troposphere, and have a large cirrus shield formed from the common cumulonimbus outflow. In many cases, these cells occur toward the leading edge of the cluster (relative to the ambient airflow), with the stratiform cloud trailing behind it. Extensive literature exists on midlatitude mesoscale convective systems, which bear some similarities to their tropical counterparts but occur in different synoptic settings (Maddox 1983).

The life cycle of tropical systems may be divided into a series of stages. First, there is a *formation stage*, in which isolated convective cells appear. These may be arranged in a line, which leads to the formation of the more rapidly moving squall line MCS, or they may be arranged more randomly. Second, in the *intensification stage,* the convective cells grow and begin to merge together. A common anvil cirrus shield forms from the combined outflow of the convective cells, along with the associated mesoscale drafts. The *mature stage* is characterized by the formation of the extensive stratiform cloud decks, which continue to precipitate actively. Finally, in the *dissipation stage*, active convection weakens and ceases. Precipitating stratiform/anvil cloud may remain for some hours afterward before finally dissipating. The full cycle is discussed in detail by Leary and Houze (1979). Each of these stages may be expected to have a distinct impact on the top-of-atmosphere longwave radiation.

b. Infrared radiative signature of convective stages

The above sequence of events may be described broadly from a more radiation-oriented point of view as follows. The system is born out of a field of low clouds, optically thick at infrared wavelengths; these merge and grow vertically into optically thick, deep convective towers reaching the tropopause and beyond; anvil clouds spread away from the cores, becoming optically thinner with distance; finally, the entire cloud system stagnates and slowly dissipates, becoming optically thinner until disappearance. The development is also evident at visible wavelengths, but this will not be considered here.

Deep convection appears in satellite imagery as areas of low T_b. Here, T_b represents the atmospheric temperature at an optical depth (from the top of the atmosphere) of approximately one. If optically thick clouds are present, this level will lie just below the tops of the uppermost cloud deck. Thin clouds will reduce T_b, but only part way toward their cloud-top temperature, giving them an infrared signature similar to that of lower and thicker cloud cover. This leads to a relatively simple identification of differing cloud types with different ranges of T_b.

1) DEEP CONVECTIVE CORES

Areas of radar precipitation echo in tropical convective clusters sampled by aircraft are usually consistent in location and size with the area in which geostationary satellite $T_b \leq 208$ K, indicating the presence of precipitating cores (Mapes and Houze 1993; Chen et al. 1996). Only optically thick cloud, deep in the troposphere, can give rise to such T_b values. In this study, the threshold T_b of 208 K is used as an indicator of deep convective cores. Such T_b values do not always overlie active convection, but when these areas are increasing with time (the situation used to identify convective onsets, see below), this should usually indicate outflow from active convection.

2) PRECIPITATING ANVILS

Much previous effort has gone into estimating rainfall from space based on infrared imagery. The area of $T_b \leq 235$ K has been found empirically to be linearly related to rainfall (Arkin 1979), though scatter in the relationship is rather large on the short timescales of in-

terest here. A similar value of 233 K was also chosen by Liu et al. (1995) to locate stratiform and deep convective cloud, on the basis of cloud-physics considerations. The correspondence between the indicator temperatures of rainfall and of stratiform anvils is not coincidental, since broad stratiform outflows are directly responsible for a significant portion of the total rainfall (Houze 1977; Churchill and Houze 1984). Accordingly, $T_b \leq 235$ K is taken here as a meaningful indicator of both optically thick, stratiform cloud regions and rainfall.

3) MIXED CIRRUS/STRATUS

Clouds produced by these systems continue beyond the zone of actual precipitation, giving rise to higher T_b as their optical thicknesses decrease. A cutoff T_b of 267 K is adopted for cloud cover associated with an MCS, following Fu et al. (1990) who used this value as the warm limit for ''cirrus anvil cloud.'' This threshold would generally include many types of mid- and upper-level cloud, since it corresponds to a temperature barely below the freezing level. In this study, therefore, regions below the 267-K threshold are considered only if they are attached to precipitating anvils ($T_b \leq 235$ K). Although the cloud thus identified is predominantly stratiform, we shall call it ''mixed cirrus,'' as it consists of ice particle clouds (often broken) whose optical thickness ranges from thin to moderately thick.

The results of this section are based on the areas C_{208}, C_{235}, and C_{267} within an MCS, defined as the areas measured in pixels whose T_b is less than the subscripted value. We identify these with the amount of convective core, core + anvil, and all cloud, respectively, associated with the system. The systems should be first identifiable as small areas of C_{208}, which then grow rapidly. At about the time that this area peaks in horizontal extent, the anvil cloud area (C_{235}) should also attain its maximum growth rate. Subsequently, the cores should dissipate, anvil cloud should peak and decline in area, and finally the mixed cirrus should dissipate. An example of a previous observation of most of the events in this sequence may be found in a case study of a convective cluster observed during the Winter Monsoon Experiment, in which successive peaks occurred in coldest cloud temperature, radar-estimated precipitation, and finally cirrus shield size (Churchill and Houze 1984, their Fig. 17).

c. Tracking method: Isolated systems

The goal of this section is to produce a quantitative description of how the evolution of these systems looks in terms of GMS T_b histograms by tracking systems. This information will provide a backdrop for the sounding-compositing effort in the next section. Unfortunately, system tracking poses significant technical difficulties that must be addressed.

The primary problem is that tropical convection occurs in complex, ever changing patterns within satellite imagery. Although it is always possible to identify aggregates of satellite pixels in an individual image that fall below a given T_b threshold [''cloud clusters,'' Williams and Houze (1987)], these aggregates do not generally maintain their individual identities in succeeding images but instead merge and split. Previous efforts to track individual systems have therefore focused on compiling size and duration statistics, using a single, defining T_b threshold (e.g., Williams and Houze 1987; Mapes and Houze 1993). An interesting and somewhat more involved, multiple-threshold method of identifying individual systems was used recently by Boer and Ramanathan (1997) for similar purposes. Our desire here to characterize the systems simultaneously at several T_b thresholds (rather than simply count systems) greatly exacerbates the identification problem.

1) SELECTION CRITERIA IN INDIVIDUAL FRAMES

To sidestep the problem, we have chosen initially to track only systems that satisfy strict ''isolation'' criteria. First, individual images are scanned to identify all ''features,'' or collections of adjacent pixels meeting one of the three temperature thresholds (diagonal pixels are not considered adjacent). A 235-K feature is taken to be an MCS and is labeled ''active'' if it contains within it subfeatures of cold cloud ($C_{208} > 0$) indicating deep convective cores. The outer limits of cloud cover associated with the MCS are taken to be the 267-K boundary.

The criteria for determining isolation of an MCS (235-K feature) are as follows. First, the 267-K boundary must not enclose any other MCS. If it does, the two are considered to be joined. Second, the MCS centroid must be distant from that of any neighboring MCS by at least $m(\sqrt{A_1} + \sqrt{A_2})$, where A_1, A_2 are the areas of the two features being considered and $m = 2$. This requirement is partially motivated by the box-counting method, described below. The third condition is that $C_{235} \geq C_{267}/q$, with $q = 3$. This condition has been included because it is clear from observing the imagery that mixed cirrus truly associated with an isolated MCS rarely exceeds the area C_{235} significantly, at least during the growing and mature stages. Violation of this condition indicates that the system is embedded in a larger area of extraneous cloud clutter, an undesirable situation. The values of m and q were set to give satisfactory results on a number of carefully inspected, trial cases.

A convenient way of visualizing the tracking procedure is to display the MCS centers on a time–longitude diagram (Fig. 2). In the figure, all active, isolated MCS centroids found in the study region are shown. Coherent systems stand out distinctly as trails of crosses at similar latitudes (indicated in the figure by cross density), the slope of which is proportional to the systems' easterly velocity—for example, the crosses marked 1–5 in Fig. 2. Infrared images of this marked feature (Fig.

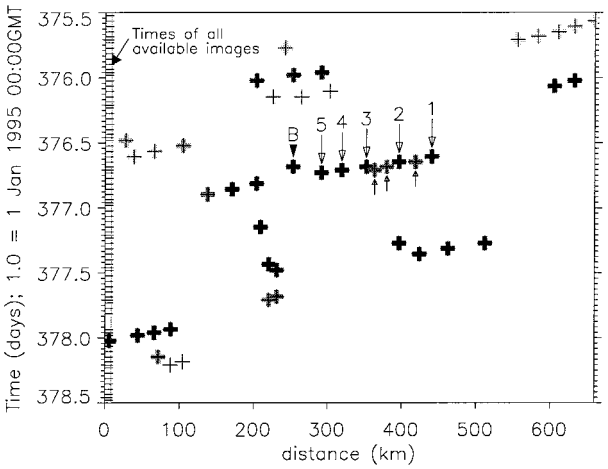

FIG. 2. Display of all active, isolated MCS centroids found in the region of study during a 4-day period (see text for these definitions). The *x* axis indicates longitudinal position within the region, the *y* axis, time. The grayscale of each cross qualitatively indicates the latitude of the system. The large, numbered arrows point to a tracked system, while the smaller arrows point to a different system at a similar longitude but farther south. The vertical row of light crosses at the left of the figure indicate times when satellite images were available.

3) show the typical progression of an isolated system through its life stages. They also show an example of a new, small system merging with the original one, showing that even the most ''isolated'' systems in the Tropics are not complete loners.

Most of the tracked systems moved with a reasonably consistent velocity during their lifetimes (i.e., trails such as those shown in Fig. 2 were generally straight), and their motion tended to be more zonal than meridional. This is not always the case with tropical systems. Most of the systems here also occurred in prevailing easterly winds throughout the troposphere, another peculiarity. Whether there is a connection between either of these facts and the isolated character of the systems, we cannot say at this time. The consistent velocities are helpful for tracking purposes, though (see below).

2) SELECTION CRITERIA AND BOX-COUNTING METHOD FOR TIME TRACKS

Any set of three or more isolated and ''active'' features spanning different satellite images (usually but not necessarily consecutive), which were subjectively determined to be the same system, were tracked as a system. Unfortunately, even the ''isolated'' systems rarely

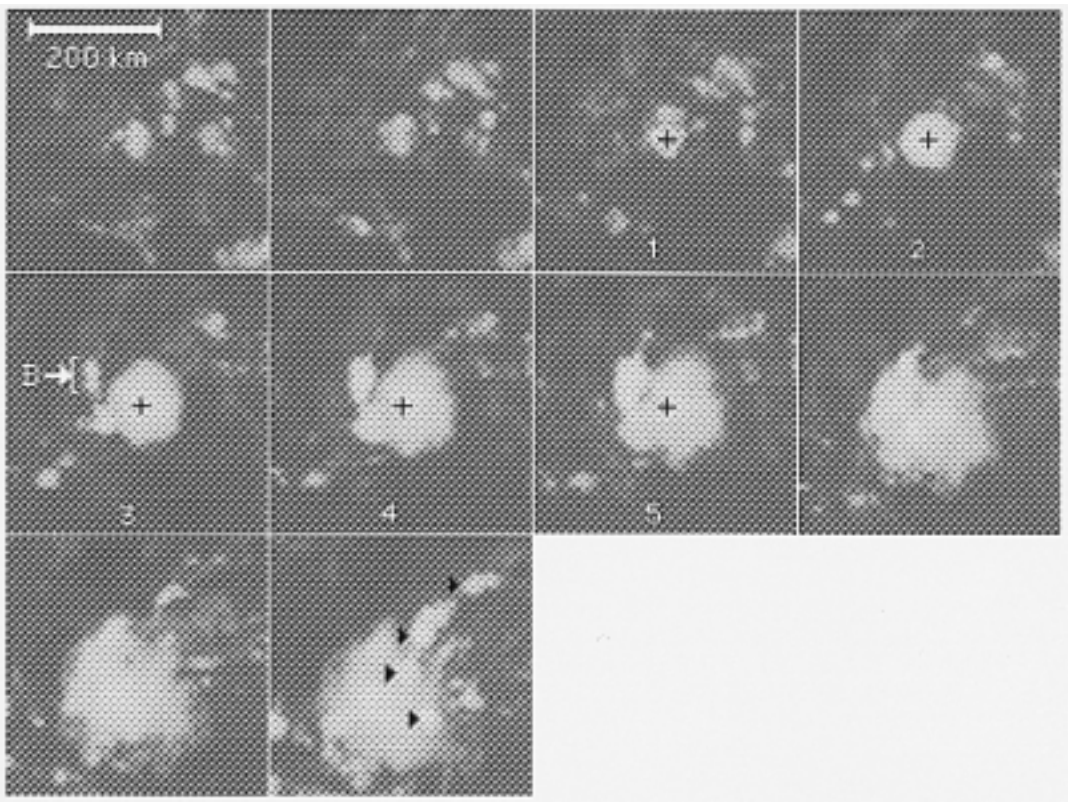

FIG. 3. The sequence of images corresponding to the system indicated by the marked trail in Fig. 2. The black crosses show the centroid position. In frame number 3, feature B corresponds to the cross in Fig. 2 marked B. This is initially a separate cloud feature that merges with the main feature in the following frame. The last frame shows the formation of several new convective cells, marked with arrows, by which time the first MCS is dissipating.

remain so for their entire lifetimes (e.g., Fig. 3). They can only be delineated by a 267-K contour in the frames in which they are isolated, but it was desired to track them throughout their lifetimes.

To achieve this, the systems were tracked by counting pixels inside a box centered on the MCS centroid. The side length of the box was set to a constant $n(C_{235}^{\max})^{1/2}$ throughout the system's lifetime, where $C_{235}^{\max}$ denotes the maximum C_{235} attained during its lifetime and n is a scale parameter. Tracking with a box of fixed size made it possible to extend the tracking 2 images prior to first identification and 10 images beyond final identification, which was done by estimating the system's propagation velocity from the nearest images in which it was identifiable and extrapolating the centroid position. This ''tracking extension'' is not too error prone due to the consistent system velocities typical of these particular systems, as mentioned above. While cloud fraction within a fixed box is susceptible to some degree of contamination from random, nearby convective activity, sufficient averaging should suppress contamination, leaving a meaningful composite. In our view, it makes more sense to regard all nearby convection as being associated with the system than it does to attempt to draw rigid boundaries around such fragile entities on the basis of satellite radiance data, even if a somewhat arbitrary ''influence distance'' must be chosen. Comparisons of the resulting composites with those obtained using the actual 267-K contour rather than a box (at the small lag and lead times that are possible with the contour-counting method) indicate that $n = 2$ gives best results. It should be noted that the motion of anvils and convective cells may be quite different, but this problem is irrelevant for T_b-histogram collection purposes during most of the life cycle as long as the active convection remains connected to its own anvils, so that all is counted. In the late stages of tracking extension, however, it is possible that the remaining anvils could be advected off in a direction different from that in which the system was traveling during its period of identifiability, which might artificially hasten the apparent demise of the anvils in the composites.

A total of 152 systems have been tracked meeting the given requirements. About half of this group were identifiable for less than 5 h, and all but one for less than 15 h (tracking extension enabled these to be tracked for between 15 and 27 h). The peak sizes ranged from 60 to 8900 pixels (1.8×10^3 to 2.5×10^5 km^2). The systems tended to occupy the smaller end of the MCS size range found in previous studies: 32% and 85% of the 208-K area in these systems was less than 10^4 km^2 and 10^5 km^2, respectively, compared with figures of roughly 30% and 75% found in previous studies (Chen et al. 1996). This is not surprising since large systems tend to be more topologically complex and are thus less likely to meet the isolation criteria. The very smallest systems were also underrepresented, with none less than 1800 km^2, since they were too short lived. It is hoped, however, that in other respects the systems tracked here were reasonably representative and that the more complicated systems may be understood on the basis of smaller and simpler ones.

d. Composite T_b profiles

To form composites, the systems have been divided into the following size classes according to their peak area attained, $C_{235}^{\max}$: those with $0 \le C_{235}^{\max} < 2000$ pixels (60 000 km^2), $2000 \le C_{235}^{\max} < 5000$ pixels (150 000 km^2), and finally $5000 \le C_{235}^{\max} < 10\,000$ pixels (300 000 km^2), containing 77%, 18%, and 5% of the systems tracked, respectively. To align the systems in time, a reference time t_o is established for each system, set to the time of peak C_{208}. Occasionally, there is more than one peak or local maximum; in these cases, the earliest peak whose amplitude is at least 20% of the largest one is used. Systems in a given size class are composited by aligning them by their respective times t_0. The system area at each time and threshold temperature is divided by the maximum achieved by the system at that temperature, and the normalized area c is averaged within each size class at each time relative to t_0. The resulting average convective system profiles are shown in Fig. 4.

As anticipated, systems are characterized by successive peaks in the cloud counts corresponding to deep convective cloud, anvils, and finally remaining cirrus. The time lags between the peaks of c_{208} and c_{235} range from 1.5 h for the smallest size class to 7.4 h for the largest, with similar delays before subsequent attainment of the c_{267} peaks. The peak in c_{235} occurs at approximately the time that c_{208} has fallen to half its maximum. The profiles tend to rise more sharply than they decay, and their duration increases markedly at the warmer thresholds and with increasing system size. Earlier studies have found similar lifetimes to those shown here (Leary and Houze 1979; Churchill and Houze 1984) and have found that larger systems last longer (e.g., Chen et al. 1996). The results here may supplement this finding by saying that all stages of the life cycle appear to grow longer with increasing size—though perhaps to greatest degree, the intermediate stage of the system where active convection is evanescing but anvil clouds are still building. Similar conclusions hold when the box size parameter n is set to one or three (results not shown), though the overall system durations tend to grow somewhat with increasing n.

The results may be compared against those from the case study of Churchill and Houze (1984) by noting that their system falls into the smallest size category here. They observed lags of 3 and 8 h, compared with 1.5 and 2.7 h here. The difference may be due either to natural variability or the fact that their cluster was sustained by land–sea contrast, which those authors suggested might extend its lifetime compared to that of a maritime system.

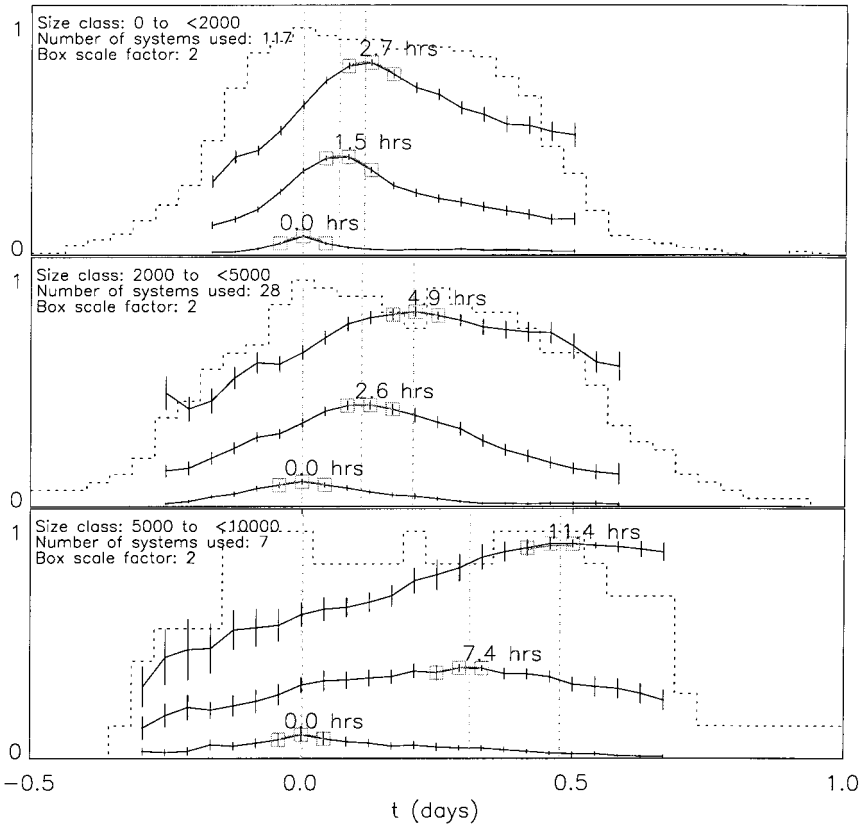

FIG. 4. Composite, normalized profiles for the area of T_b less than 208 K (bottom solid trace), 235 K (middle), and 267 K (top), as a fraction from zero to one. The horizontal axis is time in days, measured from t_0. Compositing technique is described in text. The gray dashed line is the fraction of all the individual systems in that size class that contributed to the pixel count at that time slot. Standard errors are shown as error bars. Peaks are located in time by fitting a quadratic to the nearest three values (shown by boxes).

4. A composite tropical MCS: Sounding observations

a. Convective state classification scheme

Now we would like to develop composite soundings at the different stages of evolution, using infrared radiance data to classify the soundings. The challenge is to recognize MCS development—by some objective method—in a time series of cloud areas obtained over the location of a sounding station. This classification must be applicable for all prevailing convective conditions, not simply the highly selective conditions for isolated convection posed in the previous section. First the problems associated with advection are discussed, then two classification schemes are described.

1) SYSTEM MOTION AND TRACKING

A time series obtained by examining a fixed area, centered on the location of the sounding launch, would be fully adequate for our classification purposes if the atmosphere were motionless. However, winds tend to be in the range 5–10 m s^{-1}, which means that the air mass observed by the sonde is of order 10^2 km away from the station a few hours before or after launch. This atmospheric motion needs to be accounted for.

System motion may be decomposed into *advection* (motion with the background wind field) and *propagation* (motion in a frame of reference that is moving with the background wind field). Since we wish to characterize an air mass before, during, and after this air mass experiences convective activity, it is imperative to move with the air mass when collecting the time series of satellite data for use in classification. Classification from such satellite series will be called *Lagrangian* classification. If, in the moving reference frame, a system ''enters'' a fixed region from the side, then the system is propagating into the region. We consider propagation to be effectively the same thing as new convection appearing at the leading edge of the system; for example, a newly convecting air mass just ahead of a squall is treated the same as if the convection had appeared from nowhere.

The ''wind field'' used for Lagrangian classification is taken as the mean wind from 850–400 hPa observed by the sounding itself. The resulting composites will

therefore be most accurate within this vertical range. The reason for the choice of this layer (in addition to these being interesting levels) is that comparison of observed winds with the tracked velocities of the systems in section 3 reveals that winds around the 700-hPa level are the most highly correlated with system motion [a finding consistent with previous studies; see Keenan and Carbone (1992)]. This means that airmass tracking fidelity is particularly important at these levels, since the ratio of propagative ''signal'' to advective ''noise'' perceived by an observer in the wrong reference frame will be lowest there.

For comparison, Eulerian classification is also performed, where data are collected from within a fixed area over the sounding site. In this case, movement of a system into the box may be due to advection as well as propagation, which means that the before/after classification could in some cases actually reflect upstream/downstream conditions in the neighborhood of a steadily convecting, moving air mass.

For both tracking methods the required time series is produced for each upper-air station by examining, in each image, the pixels within a box of constant side length L, which is centered on the sounding site at launch time, beginning 6 h before and ending 6 h after launch. We again calculate normalized areas $c^L_{208}(t)$, $c^L_{235}(t)$, and $c^L_{267}(t)$, this time dividing the cloudy area C by the box area L^2 to obtain the fraction of cloud cover within the box, c, where L ranges from 5 to 100 pixels (or box areas from approximately 750 to 300 000 km^2). Relative to the sounding launch times, count fractions are available at $\delta t = \{\ldots, -2.5, -1.5, -0.5, +0.5, +1.5, \ldots\}$ hours (the extra images available at -1 h are not used, because they cause the onset statistics to become nonstationary and do not contribute significant additional information).

2) Convective pattern recognition

Different analysis methods of varying complexity can be employed for the task of recognizing the stage of convective development from the time series $c(t)$. The simple approach of identifying convective systems by their onset and termination using c_{208} alone has been adopted here. This strategy exploits the relative brevity of the active stage of convection compared with the subsequent stages (which reduces the value of the latter in establishing the timing of events).

Sounding classification begins by identifying *convective onsets.* A convective onset occurs when $c_{208}(T) > 0.1$ at time t but not at any other time within the previous 3 h. The adoption of the critical fraction 0.1 follows Fu et al. (1994), but the results were not sensitive to this choice as long as it was not too large. The choice of 3 h as the defining time lag was motivated by the decay times evident in Fig. 4 but was also used by Frank (1978). Similarly, a convective *termination* is defined as the first occurrence of $c_{208}(t) < 0.1$ after an onset. Note that by this definition, anvil clouds will still be present and the MCS will not yet have disappeared.

TABLE 1. Stages of development.

No.	Stage	Conditions
0	Nonconvective	$c^L_{208} < 0.1$ within 3 h
1	About to occur	Onset next 3 h
2	Just started	Onset previous 3 h
3	On going	$c^L_{208} > 0.1$ within 3 h
4	About to finish	Termination next 3 h
5	Just finished	Termination previous 3 h

Each sounding was then assigned two classifications: a stage of development and a time from onset δ_{on}. The six stages of development are defined in Table 1. Stages two through six correspond roughly to the stages described qualitatively in section 3a, while stages zero and one correspond to nonconvective and preconvective conditions. The tiny number of soundings not falling into any of these categories (i.e., where termination immediately follows onset, or vice versa) were not assigned a stage.

Interval δ_{on} was established as the time since the most recent onset; or, if there had been no onsets during the previous 6 h, the negative of the time until the next onset. That is, δ_{on} was the time at which the sounding occurred, relative to that of the onset. If no onsets occurred within 6 h, then δ_{on} was not assigned.

It may at first seem unjustified to use information from an extended area in classifying a sounding that is essentially a point measurement. However, the point measurement may correctly be regarded as a noisy observation of the area mean over the satellite counting box—provided that ''noise'' is understood in this case to include all variability at scales smaller than the box, in addition to actual instrument error. We assume that both noise sources are independent of the signal, contributing nothing to the composites in the large-sample limit (except possibly instrument biases). The catch, of course, is that the technique is unable to measure accurately the true *scatter* or variability of the areal mean, no matter how large the sample, since the observed scatter includes a noise component that is unknown and rather large. Nonetheless, the observed scatter may still be informative as a bulk indicator of both forms of variability (see below).

b. Sounding composites, 120 × 120 km

We have composited all soundings according to both their stage and t_{on}, with Eulerian and Lagrangian tracking, over a range of box sizes. Composite sounding variables may be plotted by stage to produce a convenient, pseudotemporal representation of the life of a convective event. They may also be plotted by t_{on} to give a genuinely temporal representation of the development within a few hours before or after convective onset. The stage 0 composite includes 3664 soundings,

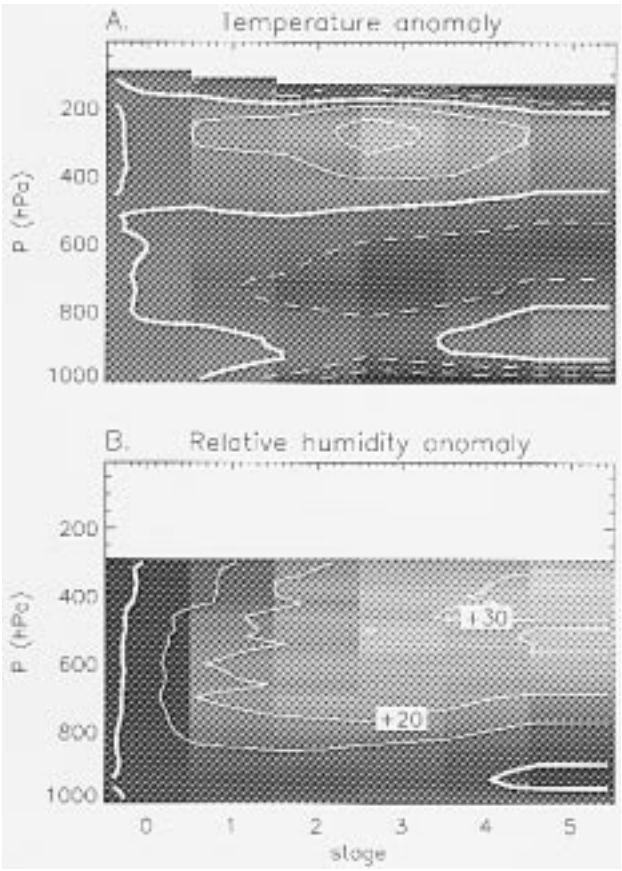

FIG. 5. (a) Mean temperature anomaly vs stage (x axis) and height (y axis), contour interval 0.5 K. (b) Mean relative humidity anomaly; contour interval 10%. In both panels, the thick contour indicates zero and negative contours are dashed. Classification is Lagrangian with $L = 21$. Anomalies are with respect to the overall mean.

and the other stages from 57 to 131 soundings each, while the t_{on} composites contain from 51 to 75 soundings each. Each set was contributed broadly from among all the stations. So in effect, the results shown below may be regarded as composites of approximately 50–100 independent convective systems, sampled randomly by the different stations, though the number of systems actually sampled is considerably greater. In this section the Lagrangian composites obtained with a counting box of 21 × 21 pixels (~13 000 km^2) are shown.

1) TEMPERATURE AND RELATIVE HUMIDITY

The mean composites of temperature and humidity are shown as anomalies from the grand mean of all soundings in Fig. 5. In these plots, signals whose standard error is greater than half the overall standard deviation are not shown. Humidities above 300 hPa are also not shown owing to instrument limitations.

The features appearing in these plots, as one goes from initiation to termination of convection, bear a very close resemblance to those found in composite studies of squall line systems as one goes from what is normally called the ''environment'' (the air moving into the squall) to the wake (the air trailing behind the squall as it propagates). On one hand this is not surprising, since propagating squalls are responsible for some of our convective ''onsets.'' On the other hand, a majority of systems encountered in previous studies have been nonsquall convective bands and cloud clusters. These have generally exhibited convective and mesoscale features similar to those of squall systems (Frank 1978; Leary and Houze 1979; Zipser et al. 1981), though the magnitudes of individual features have varied, and measurable modification of the boundary layer (for example) has not always been observed (e.g., Zipser and Gauthier 1978). It is interesting that the profiles here should nonetheless resemble a squall cross section so closely.

The features appearing in Fig. 5 include the following.

- Cooling of up to 1.5 K below 950 hPa once convection is under way due to cold convective downdrafts (Zipser 1969; Houze and Betts 1981). During the peak convective stage (3), cool anomalies extend to some degree throughout the boundary layer.
- Slight warming from 800 to 950 hPa as the convective event terminates. This is probably due to unsaturated descent in the mesoscale downdraft of the stratiform region of an MCS (Gamache and Houze 1985; Johnson 1986).
- Cooling of up to 1.2 K in the lower to midtroposphere. This is centered near 725 hPa initially, rising to 600 hPa by the termination of the event. This cooling pattern has been attributed to evaporation of stratiform precipitation (Gamache and Houze 1985); however, some studies have not found cool anomalies (e.g., Mapes and Houze 1992) or have even found warming tendencies under the stratiform regions (e.g., Johnson 1986). Furthermore, here it appears to bracket convection, as it is present even at stage 1. The temperature anomalies are apparently heterogeneous in space and may vary depending on the type of system (Gamache and Houze 1985).
- Warming of up to 1.3 K in the upper troposphere. This is centered around 250–275 hPa initially, descending very slightly during the course of the event, and also brackets the development of convection. The bipolar temperature anomaly (having opposite sign in the upper and lower levels) in the free troposphere is associated with a similar bipolar pattern in mesoscale drafts in the wake of the MCS convective zone.
- Cooling above 175 hPa of up to 1.0 K once convection is under way. Possible physical mechanisms for this are dry-adiabatic ascent above cloud top forced by the mesoscale updraft (Fritsch and Brown 1982; Gamache and Houze 1985) or cloud-top radiative cooling (Johnson and Kriete 1982). The latter seems unlikely to be the dominant cause, given the rapid development of the anomaly shown in Fig. 5a.

- Elevation of relative humidity (RH) in almost the entire observable troposphere. Below the boundary of the lower to midtropospheric cooling anomaly, this moist anomaly is a constant 5% RH or so in stages 1–4; above the boundary, the moistening is greater than 5%, and is particularly pronounced in the upper levels. These effects are common knowledge, with midlevel relative humidity being a likely aid to convection (e.g., Nicholls et al. 1988) and upper-level moisture a consequence of convective transports and detrainment (e.g., Soden and Fu 1995) as well as any lifting that may accompany the convection. Increases in RH do not reliably correspond to increases in specific humidity however (see below).
- Drying at 850–950 hPa in stage 5. This feature, discussed by Zipser (1977), apparently results from low-θ_e environmental air that enters the mesoscale anvil region (without first having interacted with convective drafts) and sinks due to evaporative cooling by stratiform precipitation.

An interesting characteristic of the figures is the general upward moving trend in the cold and moist anomalies. One would expect to find this in the part of the signal contributed by squall lines, since these lines tend to tilt sharply away from their direction of propagation. The trend does not appear clearly in the composite studies of Frank (1978) or Barnes and Sieckman (1984), however, perhaps due to their small sample size. Upward propagation of anomalies in wind divergence (Tollerud and Esbensen 1985) and vertical velocity (Frank 1978) are easily seen in past studies, and composites of the easterly wave show the trend in thermodynamic fields (Reed and Recker 1971). Models have replicated this feature in their thermodynamic fields as well (Lau et al. 1993).

Another interesting feature of Fig. 5b is that the humidity and temperature anomalies are significant even at stage 1, or *before* the onset of convection. This is especially true of midtropospheric RH, which is about the same at stage 5 as at stage 1. This is shown more clearly later in Figs. 7a,b, which show the mean RH from 700 to 400 hPa as a function of stage and t_{on}, respectively. The RH anomaly begins before the onset of convection (Figs. 7g,h show the composite c values on the same timescale as the soundings) and precedes the onset by at least a few hours (Fig. 7b). This indicates that convection was much more common in locations that were already moist in the midtroposphere. Interestingly, the opposite anomalies appeared before convection in GATE data (Frank 1978).

2) Sensitivity to airmass tracking

It has been argued that convection should be monitored in a frame of reference that moves with the air mass, rather than being fixed to a station, in order to observe temporal behavior properly. Unfortunately, atmospheric shear makes it impracticable to do this in a way that yields correct results at all levels (one would have to classify data separately at each level using the winds at that level, then blend the results, an onerous task). The single-wind tracking method used here must be regarded as approximate, with worsening errors as one approaches the upper troposphere and possibly the surface. The magnitude of error likely in the composites as a result of this problem may be estimated by examining the differences between the Lagrangian and Eulerian composites.

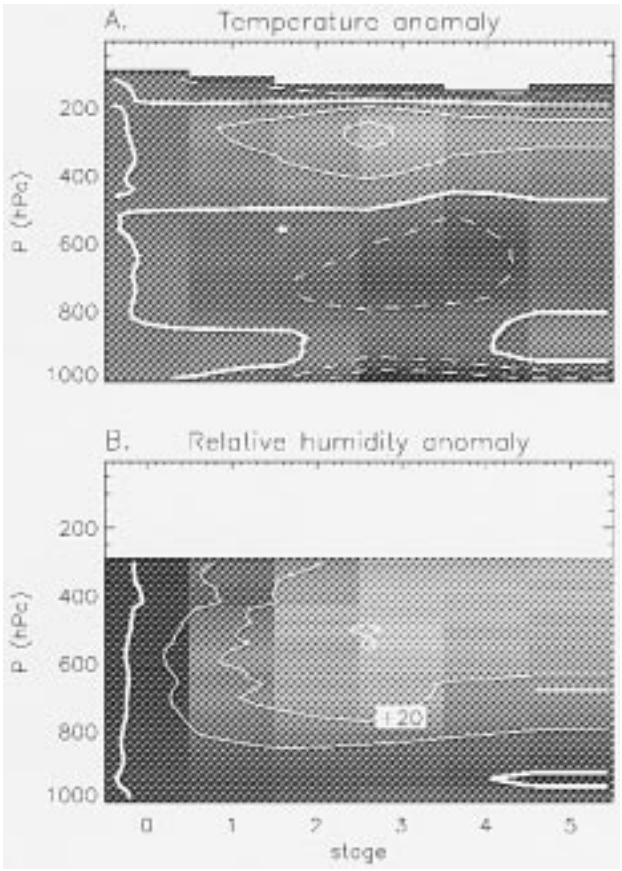

FIG. 6. As in Fig. 5 except for Eulerian classification.

The Eulerian composite for $L = 21$ pixels appears in Fig. 6. The composites in the actively convective stages do not differ perceptibly from those of Fig. 5, but some differences at stages 1 and 5 are noticeable. The Eulerian classification shows a more long-lived upper-tropospheric temperature anomaly at stage 5 but less long-lived upper-tropospheric humidity and midtropospheric temperature anomalies. Also, the dry minimum above the boundary layer is weaker. The mid- and lower-tropospheric differences are probably the result of contamination by samples of air masses downstream from the ones containing convection, but the upper-tropospheric difference is hard to interpret. The stage 1 composite shows slightly weaker signals overall than with La-

grangian compositing. Fortunately the differences are not large, but the true upper-level signal at stage 5 must still be regarded as somewhat uncertain.

Most of the remaining results in the paper employ Lagrangian classification. Anyone wishing to test a numerical model against these results, however, would probably prefer to use the Eulerian composites, since it is a lot easier to extract time series at individual model locations without having to track air masses. The reasonable resemblance between the two composites means that an informative signal can still be obtained by this method.

3) ATMOSPHERIC STABILITY

One way of quantifying explicitly the convective stability changes implicit in Fig. 5 is by calculating convective available potential energy (CAPE) and convective inhibitive energy (CIN). There is no doubt from previous studies that CAPE drops dramatically with the passage of a tropical squall, as warm, moist boundary layer air is replaced with cold air from convective downdrafts. But the relationship between CAPE and convection is less clear when averaged over scales from the mesoscale on up—a matter of considerable interest in modeling large-scale behavior. Previous results relevant to larger-scale relationships include documented loss of CAPE in deep-convective case studies (Mapes and Houze 1992), in the trough of equatorial waves (Thompson et al. 1979), and recently in the aftermath of sustained westerly wind bursts in the tropical Pacific (J. Fasullo 1998, personal communication).

CAPE is calculated here by integrating the net mechanical work done by an air parcel from near the surface, during ascent from its initial level to the first level above 600 hPa at which it is neutrally buoyant. CIN is the integral of the work required to lift the parcel to its level of free convection, or 600 hPa, whichever is lower. Both quantities are usually positive in the tropical western Pacific, but CAPE by this definition can be negative if the positive area in the thermodynamic sounding is less than the CIN. The CAPE (CIN) is a decreasing (increasing) function of the starting altitude of the parcel; results given here show the average of CAPE associated with parcels starting from 1000 to 900 hPa, which is denoted ACAPE to distinguish it from the energy of a 1000-hPa parcel alone which is sometimes used. Values of the latter, denoted CAPE_{1000}, will be shown here for comparison, but calculated using only the reef/small island soundings [see section 4b(4) for further explanation]. A floor value of -99 J kg^{-1} is established for either form of CAPE, since values for stable soundings are sensitive to the definition and difficult to interpret, and a ceiling of 500 J kg^{-1} for CIN is established, which is only attained by some of the absolutely stable soundings. Reversible, adiabatic ascent is assumed, with 50% of condensate freezing to ice at -10°C. Standard, pseudoadiabatic assumptions would yield results approximately 100–300 J kg^{-1} higher than those shown for the 1000-hPa parcel.

Since CAPE and CIN have heavy-tailed distributions (i.e., most instances cluster loosely around a central value, but some—far more than in a Gaussian distribution—stretch out to much higher values), and since the extreme high (low) values for CIN (CAPE) are somewhat arbitrary, a statistic called the ''biweight mean'' will be employed to characterize the typical value of these and other observables from an ensemble of measurements. The biweight mean is given by

$$\overline{X}_{\mathrm{bi}} = M + \left[\sum_{i=1}^{n} (X_i - M)(1 - u_i^2)^2\right]\left[\sum_{i=1}^{n} (1 - u_i^2)^2\right]^{-1},$$

where M is the ordinary mean, X_i is the value for observation i, and u_i is a sort of inverse weight for this observation, equal to the ratio of the observation's absolute difference $|X_i - M|$ to the mean of this absolute difference over all the observations, multiplied by the factor 1/7.5 (which previous studies have recommended for optimum performance), with a maximum weight of 1.0. This statistic combines the robustness or efficiency of estimation of the mean, with the resistance to outliers of the median. See Lanzante (1996) for more information. The 95% confidence intervals are computed using bootstrap sampling with corrections for bias and acceleration (the so-called BcA method). Bootstrap samples are simulated data samples obtained by randomly choosing from the available samples, allowing multiple selection of the same one; the distribution of simulated biweight means from 2000 bootstrap samples is used to estimate the range of true values that could have led to the observed sample. The BcA corrections to this are required by the asymmetry of the distributions. Space does not permit a fuller description; please see Efron and Tibshirani (1993). Figures in this paper also show the ordinary mean and median values for comparison, which generally exhibit similar behavior.

The statistics of the ACAPE ensembles are plotted versus stage and versus time in Figs. 7c,d, respectively. Each statistic shows a rapid, smooth drop in CAPE_{1000} and ACAPE beginning with the onset of convection, decaying with a time constant of order 2–3 h (see section 4c for further discussion). A more dramatic drop occurs in the $L = 5$, Eulerian composite (Fig. 8). This plot represents the changes in ACAPE seen by a fixed observer due to local (15-km radius) changes in convection. This drop is still not as sharp as one might see in highly detailed in situ observations of a passing squall line, but this may be because not all forms of convection exhibit such sharp behavior. In any case the result shows that the technique's resolving power is reasonably good. Final ACAPE is typically less than half of the initial value, with the decrease being highly statistically significant. CAPE_{1000} behaves similarly, though the decline is slightly smaller in relative terms.

Some of the consumption of CAPE is associated with

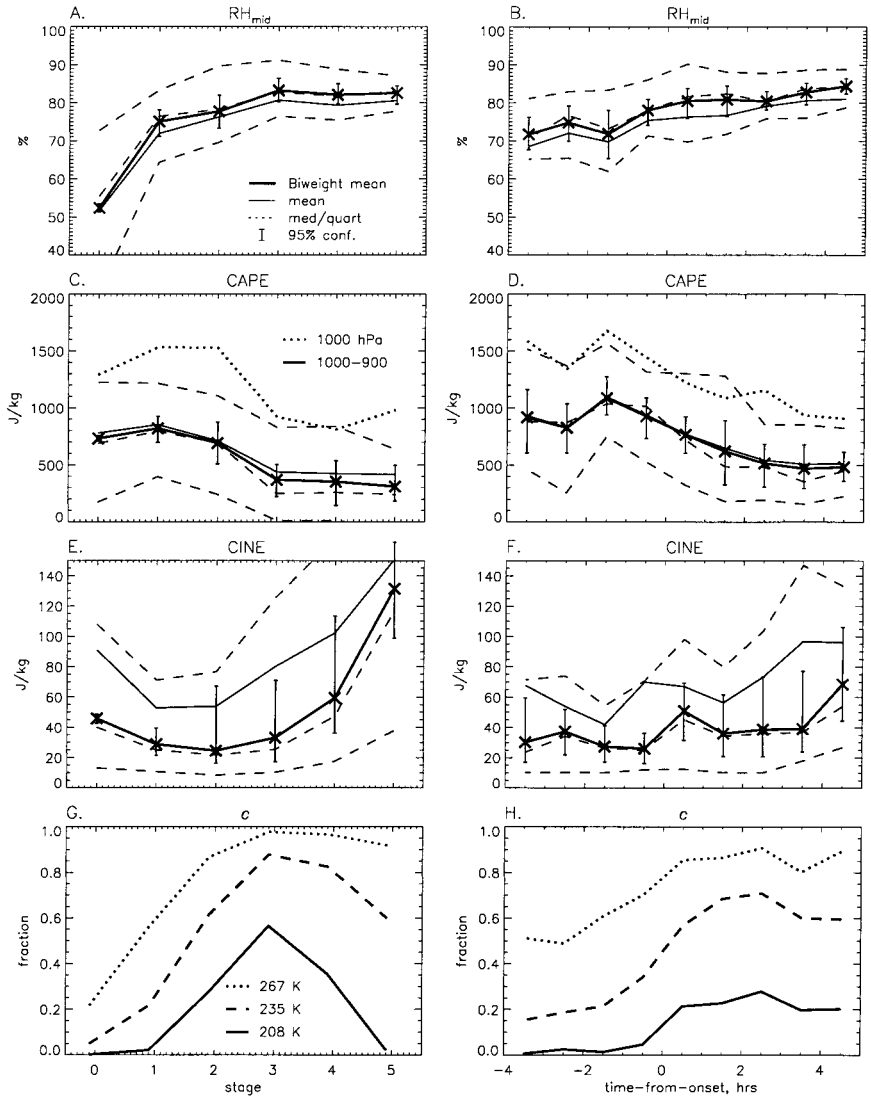

FIG. 7. Lagrangian-composite variables using a 21 × 21 pixel box. (a) Midlevel RH vs stage; (b) RH vs t_{on}; (c), (d) as in (a), (b) except ACAPE; (e), (f) as in (a), (b) except CIN; (g), (h) as in (a), (b) except cloud fractions as indicated. In (a)–(f), heavy solid line indicates the biweight mean (see text for description); light solid line the arithmetic mean; dashed lines the 25th, 50th (median), and 75th percentile or interquartile levels; error bars, the 95% confidence intervals for the biweight mean. In (c), (d), the heavy dotted line shows the biweight mean of CAPE calculated using a 1000-hPa parcel.

the deep upper-tropospheric warm anomaly from Fig. 5a, but most comes from decreases in boundary layer θ_e. This is also exhibited in the CIN (Figs. 7c,d), which reaches a minimum at the time of maximum growth of convection, followed by a steady increase to levels above 100 J kg^{-1} by the end of the event. It is interesting that, even though CIN does not build for several hours and becomes very high only after convection has terminated, CAPE has already fallen somewhat before convective activity peaks. Soundings taken just before the onset of convection (stage 1) show only two-thirds of the CIN of soundings not followed by convective onset (stage 0), suggesting that CIN decreases first, followed by simultaneous CAPE decreases and convective growth, then convective decay and CIN growth.

The CIN growth is not associated with changes in the θ_e lapse rate within the boundary layer though, as one might expect. Profiles of θ_e at each stage, shown in Fig. 9, indicate that the warm and moist anomalies shown earlier in the lowest few kilometers act to produce θ_e changes that are nearly uniform in the vertical. The increasing CIN comes purely from the changes in temperature, which are largest near the surface.

Another interesting feature of Fig. 7, not explored in previous compositing studies, is that the variance of CAPE decreases markedly with the progress of con-

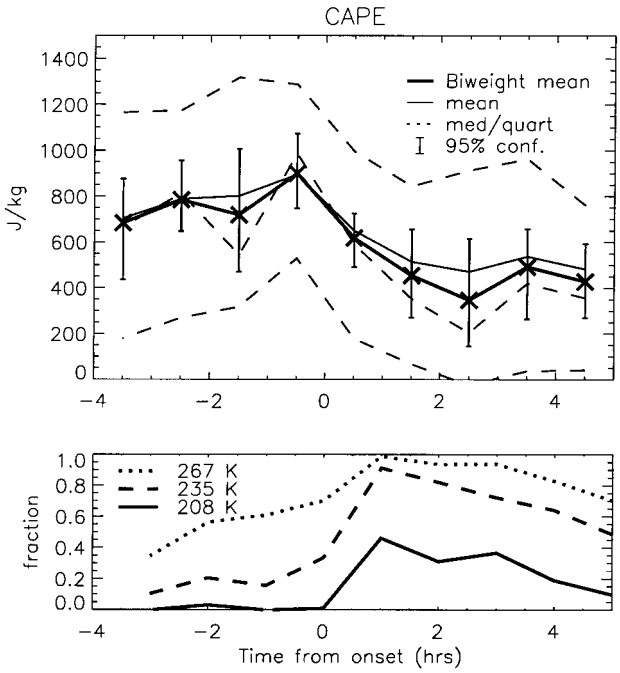

FIG. 8. (top) As in Fig. 7d and (bottom) as in Fig. 7h except for Eulerian classification with $L = 5$. $CAPE_{1000}$ not shown.

vection. This is not caused by boundary layer θ_e variance, which does not change significantly either with time or height through stages 1–5 (for which reason individual interquartile ranges from these stages have been left off the figure for clarity, their overall mean being indicated instead). Part of the narrowing of CAPE is an artifact of the way it is calculated, since the limits of integration increase with the value of the integrand, causing mean and variance to scale together. However, it turns out that some of the narrowing of CAPE is physically significant, arising from an increase in the positive correlation between subcloud-layer moist energy and temperatures aloft—a linear statistic independent of the CAPE calculation issues. The correlation between θ_e (integrated from 1000 to 900 hPa) and temperature (integrated from 900 to 200 hPa) increases from $+0.15$ ($\pm$standard error 0.02) among stage 0 samples to a peak of $+0.46 \pm 0.13$ at stage 4. These values are not sensitive to modest changes in range of integration. The increasing correlations indicate that convection acts not only to reduce the buoyancy of near-surface air parcels, but to modify the subcloud layer in a way that depends on temperatures aloft (or the reverse, or both). This result provides a bit of additional evidence for the idea, often employed by modelers, that convective effects increase systematically with the initial instability in the manner of a negative feedback.

4) WIND

The development of the wind field in the environment of tropical convective systems consists primarily of the generation of midlevel vorticity, low-level convergence, and upper-level divergence (e.g., Leary and Houze 1979). Our sampling strategy is not conducive to observing these wind anomalies, since they are spatially complex and involve horizontal derivatives. However, wind speeds and shear can easily be composited. Relationships between surface wind speed and convection have received considerable attention owing to their potential importance in ocean–atmosphere coupled behavior (e.g., Zhang et al. 1995). Their behavior with the progression of convection as obtained from about three months of shipboard data was reported for the TOGA COARE period by Young et al. (1995), who found large increases in surface fluxes during convection that were caused primarily by strong winds.

Figure 10a shows the stage plot of 1000-hPa wind speed, using observations only from stations that were located within 15 m of sea level on reefs or small islands: Yap, Truk, Kwajalein, Majuro, and Tarawa. The winds at stage 3 (ongoing active convection) turn out to have been about 30% higher than at other times, with little variation through the other stages. This is similar to the signal obtained by Young et al. (1995) for the COARE intensive observation period (IOP) but smaller

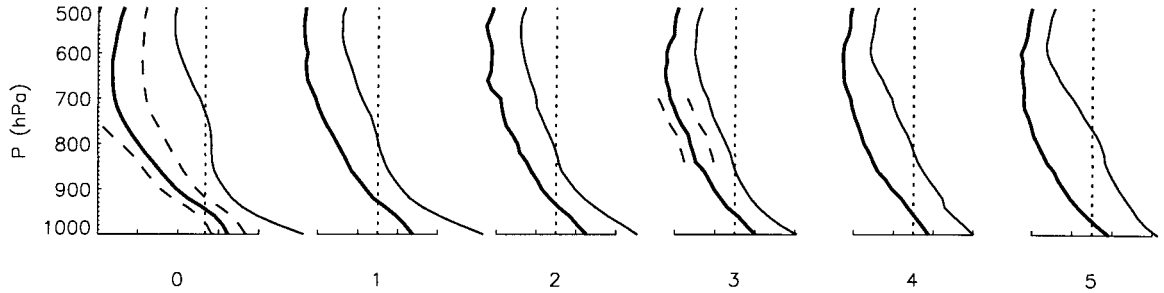

FIG. 9. Lower-tropospheric θ_e (thick lines) and θ^*_e (thin line) profiles at each stage. Horizontal axes have tick marks every 5 K and vertical dotted lines indicating the 350-K level in each panel. Solid lines show the biweight means; dashed lines show the 25th and 75th percentile levels of θ_e only. To avoid clutter, the short sections of dashed line drawn on the stage 3 panel indicate the mean deviation of these curves from the biweight mean, over all levels shown and all stages from 1 to 5, since differences within this domain were small and statistically insignificant.

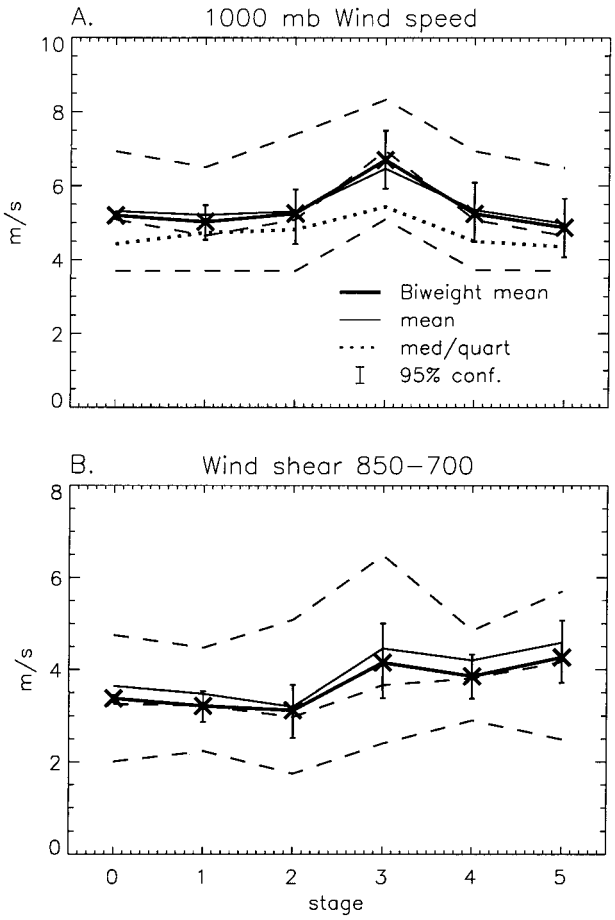

FIG. 10. (a) The 1000-hPa wind speed from reef/small island stations. Heavy dotted line shows the biweight mean wind from all stations. (b) Wind shear (absolute value of the vector difference between the wind at 850 and 700 hPa) from all stations.

than, and of different character from, the signal they obtained from the COARE pilot cruise (which collected only 3 weeks of data). When data from the larger island stations were thrown in, the signal became smaller and the spread in values (not shown) grew slightly, suggesting that these stations give unreliable surface winds. The size of the 95% confidence intervals in Fig. 10a indicates that the 30–50 systems effectively sampled here by the small island/reef stations were about the minimum number necessary for clearly resolving a climatologically meaningful signal.

Wind shear is also intimately coupled with convection. Convection influences large-scale behavior by transporting momentum and generating mesoscale pressure fluctuations (LeMone et al. 1984), and convective development is itself influenced by environmental shear (Barnes and Sieckman 1984; Nicholls et al. 1988). The shear at boundary layer top (absolute value of the vector difference between the winds at 850 and 700 hPa) is shown in Fig. 10b. It increased by about 25% during mature convection, then remained elevated thereafter. Previous work has shown that, while shear parallel to a convective line is damped by the convection, perpendicular shear can be generated (LeMone et al. 1984). The latter process could be responsible for the overall increase in shear shown here. Unfortunately, we cannot explore the issue further with this dataset since neither the direction of propagation nor the orientations of the sampled systems can be identified objectively, especially since not all systems are convective lines. The shear components parallel and perpendicular to the mean wind were checked, however (not shown), and were found to show similar increases.

5) COLUMN ENERGY

The large sample size in this study makes it possible to estimate the net change in column energy during the course of a convective event. It is known that moist static energy, or MSE (composed of latent heat, enthalpy, and potential energy), is exported horizontally from convective systems due to the concentration of lifting above about 600 hPa, where the MSE profile increases with height; this is particularly true within stratiform regions at the later stages of convection (Mapes and Houze 1995). It is not obvious where the energy comes from. Since ''convective heating'' is not a source of MSE (it is simply the conversion of latent heat into enthalpy), the exported energy must be supplied by some combination of either (a) depletion of MSE stored within the column or (b) convergence of radiative and convective energy fluxes through the upper and lower boundaries (see Neelin and Held 1987).

At the lower boundary (surface), previous observations (Young et al. 1995; Geldmeier and Barnes 1997) have shown that net upward fluxes of sensible and latent heat increase substantially during and after convection. In the present study direct observations of these fluxes are not available, nor do we have sea surface temperature observations at island stations (or even a sea surface for that matter). This notwithstanding, ''pseudoflux'' anomalies have been estimated here by linearizing the bulk formulas of Liu et al. (1979) for typical conditions, neglecting surface temperature variations, using 1000-hPa observations, and assuming mean actual fluxes of 100 and 10 W m^{-2}, respectively, for latent and sensible heat. Specifically this means that latent heat flux is taken to decrease as 1000-hPa specific humidity increases, at 20 W m^{-2} kg g^{-1}; the combined flux decreases as 1000-hPa temperature increases, at 10 W m^{-2} K^{-1}; and both are proportional to the wind speed. The resulting total flux anomalies (latent + sensible) for each stage are shown in Fig. 11 using only the reef/small island stations. The signal is a primarily wind-driven increase of 50 W m^{-2} during the ongoing convection stage, which decays slowly back to the background level. The slower decay is because of cooler air temperatures enhancing the fluxes, but in real life cooler oceans might mitigate this effect. This signal is a bit

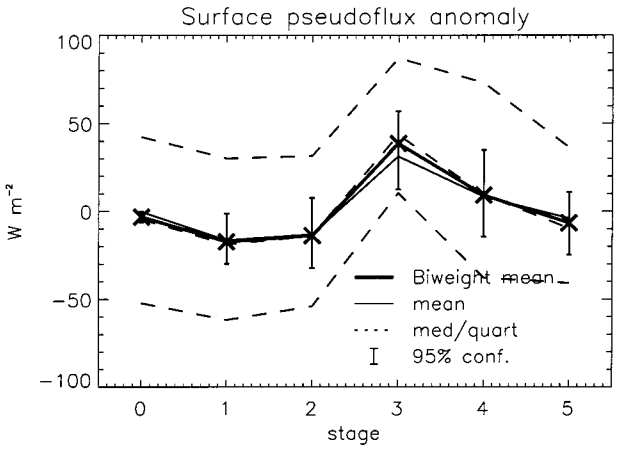

FIG. 11. Pseudoflux anomaly from the mean, estimated from 1000-hPa properties at reef/small island stations according to linearized bulk formulae at fixed SST.

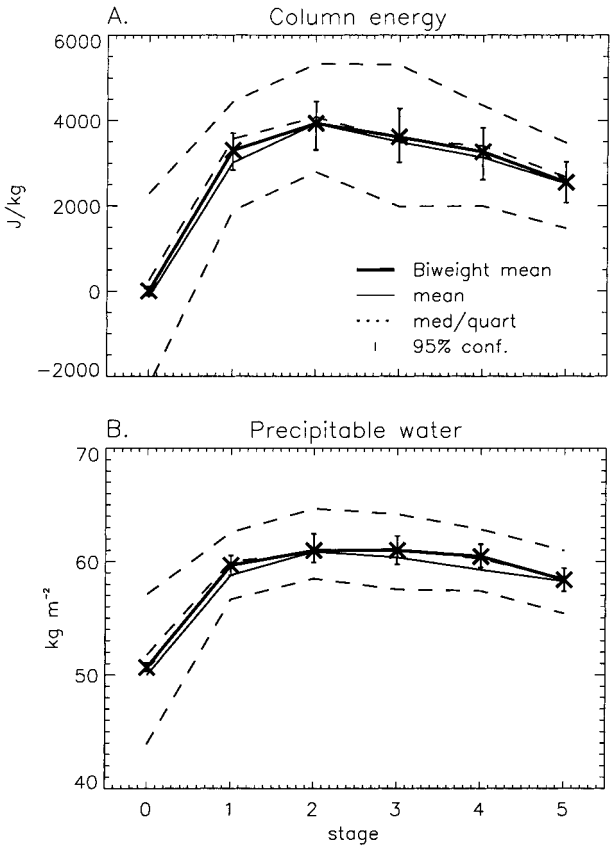

FIG. 12. (a) Column-integrated moist static energy anomaly at each stage, from Lagrangian $L = 21$ composites. (b) Precipitable water.

smaller than the COARE IOP result of Young et al. (1995), which is probably more reliable, but the difference is not large. Significantly larger increases have been reported in at least one individual case (Geldmeier and Barnes 1997).

Vertical convergence of radiative fluxes also increases during convection. Cloud cover reduces outgoing infrared radiation by much more than it does the net upward infrared at the surface, increasing convergence into the column by up to 100 W m^{-2} (about 1 K day^{-1}) or more. Solar absorption in clouds adds further energy during daytime, in amounts perhaps equal to as much as half of the additional longwave convergence when diurnally averaged (though exact amounts are a topic of debate at this time). Thus the combined energy input into the actively convecting region could be up to 2 K day^{-1}; over a typical convective event from stages 1 to 5, one might reasonably expect a total energy input anomaly from radiative and surface fluxes of perhaps 200–600 J kg^{-1}.

Despite this energy influx, the column energy content decreases during convection by some 800 J kg^{-1} or more (Fig. 12a). It is calculated here by integrating the MSE from the surface to 120 hPa (the signal is not sensitive to the choice of upper boundary). Most of the signal is contributed by the column-integrated latent heat, which is proportional to precipitable water (Fig. 12b). Both variables are substantially larger before convection than they are in the absence of convection; they then increase slightly further before finally receding to just below their initial levels. The total energy signal is larger than the precipitable water signal, owing to a drop in the column enthalpy. Column potential energy changes are small. Each of the three forms of energy increases in the upper troposphere and decreases in the lower, so as to yield a relatively small net change.

The *decrease* of precipitable water during convection may seem surprising in light of the oft-noted increases in relative humidity accompanying tropical convection through most of the troposphere. The decrease results from three factors: first, the greatest RH anomalies are in the upper troposphere, which contributes little to the column total; second, the temperature anomalies throughout the lower troposphere (where most of the moisture is) mean the specific humidities are lower, even though the RH may be slightly higher in some places; third, the bulb part of the ''onion'' sounding appearing in the wake of convection (Zipser 1977), albeit confined to a small vertical extent, represents a significant decrease in total water. Both variables presumably continue to decrease smoothly as the anvils dissipate, eventually returning to the stage 0 values.

The area-average temperature changes are relevant to simple theories of tropical moist dynamics. Some theories view convection as a driver of large-scale motions, while others view it as either a damper of these motions or a neutral response that simply changes the effective stratification (see Emanuel et al. 1994; Yu et al. 1998). The question of growth or decay turns on whether convective heating leads or lags large-scale ascent, which would be observed, respectively, as positive or negative temperature anomalies during convection. The actual picture is a little more complicated (Fig. 5a), since the

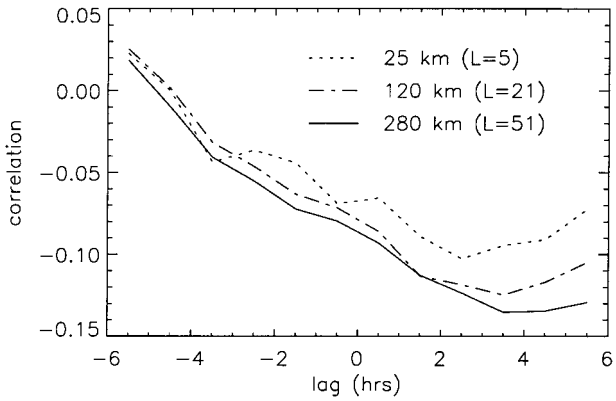

FIG. 13. Lag correlation between c_{208} and ACAPE, with the right side corresponding to CAPE anomalies that lag behind c_{208}. Dotted, dot–dash, and solid lines indicate 5×5. 21×21, and 51×51 pixel cloud counting areas, respectively.

anomalies are strongly height dependent. When vertically averaged or projected onto the fundamental vertical (sinusoidal) mode, an overall cooling trend has clearly appeared by the final convective stage, but in the earlier stages this signal is ambiguous [for further discussion of vertical modes see Mapes and Houze (1995)]. Below 500 hPa, however, cooling prevails at all stages including preonset. Thus the data are consistent with damping of wave modes whose vertical motion is concentrated below 500 hPa. The effect on, say, the fundamental vertical mode is less clear, but mild damping looks possible as long as the wave period is long compared not only to the timescale at which CAPE is consumed (see below), but also compared to the duration of a typical MCS (which is several times longer). It should be noted that virtual temperature effects on buoyancy, though fairly small, will enhance the net loss of buoyancy at low levels and gain at high levels. A good summary of recent ideas on the interaction of convection and large-scale dynamics may be found in Smith (1997).

c. Sensitivity to horizontal scale

The compositing process has been repeated using a range of box sizes for classification. The stage composites do not show significant trends with horizontal scale, except plots of cloud fraction (not shown), which become smoother with slower changes and weaker composite maxima as one goes to longer length scales. At some sufficiently large length and/or time scale, stage plots of CAPE might be expected to flatten out as tropospheric quasi-equilibrium takes hold (Brown and Bretherton 1997), but they show no sign of doing so up to the 280-km scale and probably well beyond.

However, the rapidity with which CAPE responds to convection does decrease with increasing length scale (compare Figs. 8 and 7d). This is shown more clearly in Fig. 13. The peaks in these lag correlations indicate the time required for ACAPE to respond to convective effects, for each length scale. These times range from about 2.5 h at $L = 5$ to 4–4.5 h at $L = 51$, with an uncertainty of an hour or less, agreeing quite well with recent results from a numerical model (Xu and Randall 1998). Data at $L = 101$ were also obtained, but due to a belatedly discovered programming error less than half the record is available, so it is not shown on the graph (though data that are available indicate that at this scale the peak extends out to between six and nine hours).

These equilibration times are roughly equal to the time lags shown in Fig. 4 between the maxima in convective cloud and all cloud (the three panels in that figure correspond roughly to boxes of side lengths $L =$ 20, 45, and 80, filled with anvils). This suggests that CAPE reaches its minimum only during the dissipation stage of convection, for a variety of sizes of system, and that the ''equilibration time'' of atmospheric deep stability that is used in some convective models is none other than the time typically required for systems of extent equivalent to the grid size to mature and begin dissipation. Why system duration and size correlate the way they do is an interesting and unanswered question.

Further work with a larger dataset and larger boxes, perhaps with some temporal averaging as well, would be of interest in pursuing these matters further.

5. Summary and conclusions

The results of this paper provide a link between the observational database that has grown out of previous field programs concerning the detailed behavior of tropical systems and the issues relevant to the interaction of convection with large-scale dynamics.

The immediate objectives of this study are basically the same as those of Frank (1978), in that composites of mean fields have been formed at various stages of convection. A novel methodology has been developed, however, in order to make use of operational data in the western Pacific. This methodology suits our underlying goal of establishing the behavior of convecting atmospheres with reasonable statistical precision, at a variety of length scales, and with some attention paid to the variability within categories. The methodology would not be favorable for differentiating between different types or regimes of convection since this cannot easily be done objectively.

The methodology requires identifying convective onsets in a sampled air mass by means of satellite-observed histograms, a process that was first tried on isolated, carefully tracked systems. Though the tracking of these systems led to one finding that has not been well documented previously—that each part of the system life cycle exhibited similar lengthening with increasing system size—this part of the study was included mainly as a double check on, and point of reference for, the subsequent compositing exercise. The time series of cloud fractions associated with sounding composites (Fig. 7g)

closely resembles those from the tracked systems (Fig. 4), and both correspond to expectations based on physical reasoning and common experience. This indicates that the compositing technique captured the life cycle of the systems reliably, though the methodology might not work as well in environments outside the western Pacific with greater vertical wind shear. The identification strategy here does not rely on establishing boundaries by means of a single T_b threshold as has been done in past satellite-based studies, which would inevitably require the distinction of convective systems even when they are so near to each other that they cannot reasonably be considered independent of one another's influence. Instead we focus on the relationships between the intensity and type of convective activity in a region and the atmospheric state there.

In general, the character of the resulting composites qualitatively mimics that of propagating squall lines. This is interesting since the composites were constructed to show temporal rather than spatial variations and represent averages over large spatial scales. Furthermore, systems were not selected to look ''classical'' or obey any other sort of criterion (at least, not for the sounding composites); these composites simply represent whatever convection came along during the approximately 160 station-months of study. The results reinforce previous findings that a variety of forms of tropical convection share the same basic elements. The results appeared similar (though not identical) regardless of whether viewed in a reference frame fixed to the lower-tropospheric air mass or to the ground, and did not degrade very much with increasing horizontal scale, indicating that the spatial extent of the convective effects was large compared with both the distances traveled by typical convective events and with their sizes.

Certain features of tropical convection are highlighted by the results. First, the destruction of CAPE during deep convection was fairly dramatic even on large scales, beginning early in the convective process, and producing exponential decay with a time constant of 2–3 h for scales of 10^3–10^4 km^2. The time constant grew with increasing horizontal scale in a manner consistent with the lengthening of the mature stages of convection of individual systems possessing similar scale. CAPE for boundary layer air parcels decayed to a base value of around 300 J kg^{-1} (700 J kg^{-1} when calculated using a 1000-hPa parcel only); ambient CAPE was about double these values, and its decline during events remained clear out to scales of at least 10^5 km^2, which should remove any remaining doubt that CAPE is a dynamically significant quantity for large-scale behavior in the Tropics (see Williams and Renno 1993; Brown and Bretherton 1997). Linear correlations between low-level θ_e and temperature aloft increased during convection, suggesting that convection was reducing not only the mean convective instability but also its variation.

Examination of the column moist static energy budget revealed that precipitable water and column energy increased sharply before, and declined modestly during, convective events. The convergence of radiative and convective fluxes into the column through the upper and lower boundaries also increases during convection. Both this energy and the lost column energy must be exported by large-scale overturning motions (not observed directly in this study). This heat export has been diagnosed in many previous studies and follows from the concentration of the systems' mean vertical motion above the minimum moist energy level (see Mapes and Houze 1995).

In comparison with previous work, the increases in surface wind shown here during convection resembled results from the TOGA COARE IOP (Young et al. 1995). The wind behavior at 1000 hPa appeared unfaithful at the larger islands, however. Our upper-air results differ from those of Frank (1978) in that here, upper-tropospheric temperature and humidity anomalies seem to precede surface anomalies and convective onset. This is worthy of further investigation.

Previous compositing studies have avoided showing statistical uncertainty; the present results, though representing a mixture of many types of systems, at least include carefully calculated confidence intervals to show the extent to which they characterize the true behavior of an ''average'' event over the period studied. In some cases, it is clear that even more data must be collected to resolve fine structure in the signal.

We hope that the composite results may be of use in developing models of tropical circulation and/or interaction between convection and dynamics, and that they may also be useful in evaluating the behavior of general circulation models, particularly vis-à-vis their cumulus parameterizations. The Eulerian analysis presented here should be quite simple to perform in a GCM and should yield more information than simply comparing the model's climate or low-frequency variability to observations. Anyone wishing to obtain the data in digital form is encouraged to contact the authors.

Acknowledgments. Part of the work reported here constitutes the second author's M.Sc. thesis at the Institute of Geophysics, Victoria University of Wellington. The authors wish to thank James McGregor for his assistance, Chia Chou and David Neelin for comments, and particularly Brian Mapes and two other reviewers whose helpful ideas and criticism greatly improved the paper. Publication costs have been generously provided by the Universities Space Research Association, Contract NAS5-32484. Sounding data were prepared and archived by the Data Support Section of the National Center for Atmospheric Research.

REFERENCES

Arkin, P. A., 1979: The relationship between fractional coverage of high cloud and rainfall accumulations during GATE over the B-scale array. *Mon. Wea. Rev.,* **107,** 1382–1387.

Barnes, G. M., and K. Sieckman, 1984: The environment of fast- and slow-moving tropical mesoscale convective cloud lines. *Mon. Wea. Rev.,* **112,** 1782–1794.

Betts, A. K., R. Grover, and M. Moncrieff, 1976: Structure and motion of tropical squall lines over Venezuela. *Quart. J. Roy. Meteor. Soc.,* **102,** 395–404.

Boer, E. R., and V. Ramanathan, 1997: Lagrangian approach for deriving cloud characteristics from satellite observations and its implications to cloud parameterization. *J. Geophys. Res.,* **102,** 21 383–21 400.

Brown, R. G., and C. S. Bretherton, 1997: A test of the strict quasi-equilibrium theory on long time and space scales. *J. Atmos. Sci.,* **54,** 624–638.

Chen, S. C., C. L. Norris, and J. O. Roads, 1996: Balancing the atmospheric hydrologic budget. *J. Geophys. Res.,* **101,** 7341–7358.

Churchill, D. D., and R. A. Houze, 1984: Development and structure of winter monsoon cloud clusters on 10 December 1978. *J. Atmos. Sci.,* **41,** 933–960.

Efron, B., and R. Tibshirani, 1993: *An Introduction to the Bootstrap.* Chapman and Hall, 436 pp.

Elliot, W. P., and D. J. Gaffen, 1991: On the utility of radiosonde humidity archives for climate studies. *Bull. Amer. Meteor. Soc.,* **72,** 1507–1520.

Emanuel, K. A., J. D. Neelin, and C. S. Bretherton, 1994: On large-scale circulations in convecting atmospheres. *Quart. J. Roy. Meteor. Soc.,* **120,** 1111–1143.

Fitzgarrald, D. R., and M. Garstang, 1981: Vertical structure of the tropical boundary layer. *Mon. Wea. Rev.,* **109,** 1512–1516.

Frank, W., 1978: The life cycles of GATE convective systems. *J. Atmos. Sci.,* **35,** 1256–1264.

Fritsch, J., and J. Brown, 1982: On the generation of convectively driven mesohighs aloft. *Mon. Wea. Rev.,* **110,** 1554–1563.

Fu, R., A. D. Del Genio, and W. B. Rossow, 1990: Behavior of deep convective clouds in the tropical Pacific deduced from ISCCP radiances. *J. Climate,* **3,** 1129–1152.

——, ——, and ——, 1994: Influence of ocean surface conditions on atmospheric vertical thermodynamic structure and deep convection. *J. Climate,* **7,** 1092–1108.

Gamache, J. F., and R. A. Houze, 1985: Further analysis of the composite wind and thermodynamic structure of the 12 September GATE squall line. *Mon. Wea. Rev.,* **113,** 1241–1259.

Gaynor, J. E., and P. A. Mandics, 1978: Analysis of the tropical marine boundary layer during GATE using acoustic sounder data. *Mon. Wea. Rev.,* **106,** 223–232.

Geldmeier, M. F., and G. M. Barnes, 1997: The ''footprint'' under a decaying tropical mesoscale convective system. *Mon. Wea. Rev.,* **125,** 2879–2895.

Houze, R. A., 1977: Structure and dynamics of a tropical squall-line system. *Mon. Wea. Rev.,* **105,** 1540–1567.

——, 1989: Observed structure of mesoscale convective systems and implications for large-scale heating. *Quart. J. Roy. Meteor. Soc.,* **115,** 425–461.

——, and A. K. Betts, 1981: Convection in GATE. *Rev. Geophys.,* **19,** 541–576.

Jabouille, P., J. L. Redelsperger, and J. P. Lafore, 1996: Modification of surface fluxes by atmospheric convection in the TOGA COARE region. *Mon. Wea. Rev.,* **124,** 816–837.

Johnson, R. H., 1986: Lower-tropospheric warming and drying in tropical mesoscale convective systems: Implications for the problem of cumulus parameterization. *J. Meteor. Soc. Japan,* **64,** 721–726.

——, and D. C. Kriete, 1982: Thermodynamic and circulation characteristics of winter monsoon tropical mesoscale convection. *Mon. Wea. Rev.,* **110,** 1898–1911.

Keenan, T. D., and R. E. Carbone, 1992: A preliminary morphology of precipitation systems in tropical northern Australia. *Quart. J. Roy. Meteor. Soc.,* **118,** 283–326.

Lanzante, J. R., 1996: Resistant, robust and nonparametric techniques for the analysis of climate data: Theory and examples, including applications to historical radiosonde station data. *Int. J. Climatol.,* **16,** 1197–1226.

Lau, K. M., L. Peng, C. H. Sui, and T. Nakazawa, 1989: Dynamics of super cloud clusters, westerly wind bursts, 30–60 day oscillations and ENSO—An unified view. *J. Meteor. Soc. Japan,* **67,** 205–219.

——, C. Sui, and W. Tao, 1993: A preliminary study of the tropical water cycle and its sensitivity to surface warming. *Bull. Amer. Meteor. Soc.,* **74,** 1313–1321.

Leary, C. A., and R. A. Houze Jr., 1979: The structure and evolution of convection in a tropical cloud cluster. *J. Atmos. Sci.,* **36,** 437–457.

LeMone, M., G. Barnes, and E. Zipser, 1984: Momentum flux by lines of cumulonimbus over the tropical oceans. *J. Atmos. Sci.,* **41,** 1914–1932.

Liu, G. S., J. A. Curry, and R. S. Sheu, 1995: Classification of clouds over the western equatorial Pacific Ocean using combined infrared and microwave satellite data. *J. Geophys. Res.,* **100,** 13 811–13 826.

Liu, W. T., K. B. Katsaros, and J. A. Businger, 1979: Bulk parameterization of air–sea exchanges of heat and water vapor including the molecular constraints at the interface. *J. Atmos. Sci.,* **36,** 1722–1735.

Madden, R., and P. Julian, 1972: Description of global-scale circulation cells in the tropics with a 40–50 day period. *J. Atmos. Sci.,* **29,** 1109–1123.

Maddox, R., 1983: Large-scale meteorological conditions associated with midlatitude, mesoscale convective complexes. *Mon. Wea. Rev.,* **111,** 1475–1493.

Mapes, B. E., and R. A. Houze, 1992: An integrated view of the 1987 Australian monsoon and its mesoscale convective systems. *Quart. J. Roy. Meteor. Soc.,* **118B,** 927–963.

——, and ——, 1993: Cloud clusters and superclusters over the oceanic warm pool. *Mon. Wea. Rev.,* **121,** 1398–1415.

——, and ——, 1995: Diabatic divergence profiles in western Pacific mesoscale convective systems. *J. Atmos. Sci.,* **52,** 1807–1828.

Neelin, J. D., and I. M. Held, 1987: Modeling tropical convergence based on the moist static energy budget. *Mon. Wea. Rev.,* **115,** 3–12.

Nicholls, M., R. Johnson, and W. Cotton, 1988: The sensitivity of two-dimensional simulations of tropical squall lines to environmental profiles. *J. Atmos. Sci.,* **45,** 3625–3649.

Reed, R. J., and E. E. Recker, 1971: Structure and properties of synoptic-scale wave disturbances in the equatorial western Pacific. *J. Atmos. Sci.,* **28,** 1117–1133.

Sherwood, S. C., 1996: Maintenance of the free-tropospheric tropical water vapor distribution. Part I: Clear regime budget. *J. Climate,* **9,** 2903–2918.

Smith, R. K., Ed., 1997: *The Physics and Parameterization of Moist Atmospheric Convection.* NATO ASI Series C, Vol. 505, Kluwer Academic, 498 pp.

Soden, B. J., and R. Fu, 1995: A satellite analysis of deep convection, upper-tropospheric humidity, and the greenhouse effect. *J. Climate,* **8,** 2333–2351.

Thompson, R. M., S. W. Payne, E. E. Recker, and R. J. Reed, 1979: Structure and properties of synoptic-scale wave disturbances in the intertropical convergence zone of the eastern Atlantic. *J. Atmos. Sci.,* **36,** 53–72.

Tollerud, E. I., and S. K. Esbensen, 1985: A composite life cycle of nonsquall mesoscale convective systems over the tropical ocean. Part I: Kinematic fields. *J. Atmos. Sci.,* **42,** 823–837.

Williams, E. R., and N. Renno, 1993: An analysis of the conditional instability of the tropical atmosphere. *Mon. Wea. Rev.,* **121,** 21–36.

Williams, M., and R. A. J. Houze, 1987: Satellite-observed characteristics of winter monsoon cloud clusters. *Mon. Wea. Rev.,* **115,** 505–519.

Xu, K. M., and D. A. Randall, 1998: Influence of large-scale advective cooling and moistening effects on the quasi-equilibrium behavior of explicitly simulated cumulus ensembles. *J. Atmos. Sci.,* **55,** 896–909.

Young, G. S., S. M. Perugini, and C. W. Fairall, 1995: Convective wakes in the equatorial western Pacific during TOGA. *Mon. Wea. Rev.,* **123,** 110–123.

Yu, J. Y., C. Chou, and J. D. Neelin, 1998: Estimating the gross moist stability of the tropical atmosphere. *J. Atmos. Sci.,* **55,** 1354–1372.

Zhang, G. J., V. Ramanathan, and M. J. McPhaden, 1995: Convection–evaporation feedback in the equatorial Pacific. *J. Climate,* **8,** 3040–3051.

Zipser, E. J., 1969: The role of organized unsaturated convective downdrafts in the structure and rapid decay of an equatorial disturbance. *J. Appl. Meteor.,* **8,** 799–814.

——, 1977: Mesoscale and convective-scale downdrafts as distinct components of squall-line structure. *Mon. Wea. Rev.,* **105,** 1568–1589.

——, and C. Gauthier, 1978: Mesoscale events within a GATE tropical depression. *Mon. Wea. Rev.,* **106,** 786–805.

——, and R. H. Johnson, 1998: Systematic errors in radiosonde humidities. A global problem? Preprints, *Tenth Symp. on Meteorological Observations and Instrumentation,* Phoenix, AZ, Amer. Meteor. Soc., 72–73.

——, R. Meitin, and M. LeMone, 1981: Mesoscale motion fields associated with a slowly moving GATE convective band. *J. Atmos. Sci.,* **38,** 1725–1750.